AIMS Materials Science, 8(5): 760–775.
DOI: 10.3934/matersci.2021046
Received: 14 May 2021
Accepted: 08 October 2021
Published: 14 October 2021

http://www.aimspress.com/journal/Materials

Research article

Nanocarriers of Eu^{3+} doped silica nanoparticles modified by APTES for luminescent monitoring of cloxacillin

João Otávio Donizette Malafatti[1,2], Thamara Machado de Oliveira Ruellas[1,2], Mariana Rodrigues Meirelles[2,4], Adriana Coatrini Thomazi[2], Carmen Greice Renda[3] and Elaine Cristina Paris[2,*]

[1] Federal University of São Carlos, Chemistry Department, Rod. Washington Luís, Km 235-C. P.676, zip code: 13.565-905, São Carlos-SP, Brazil
[2] Nanotechnology National Laboratory for Agriculture (LNNA), Embrapa Instrumentação, XV de Novembro St., 1452, zip code: 13560-970, São Carlos, SP, Brazil
[3] Federal University of São Carlos, Department of Materials Engineering, Rod. Washington Luís, Km 235-C. P.676, zip code: 13.565-905, São Carlos-SP, Brazil
[4] Institute of Chemistry, University of São Paulo, Av. Trab. São Carlense, 400, zip code: 13566-590, São Carlos-SP, Brazil

* **Correspondence:** Email: elaine.paris@embrapa.br.

Abstract: Drug nanocarriers have been continuously improved to promote satisfactory release control. In this sense, luminescent materials have become an alternative option in clinical trials due to their ability to monitor drug delivery. Among the nanocarriers, silica stands out for structural stability, dispersibility, and surface reactivity. When using ceramic nanocarriers, one of the challenges is their interaction and selectivity capability for organic molecules, such as drugs. In order to overcome such adversity, superficial modifications can be carried out to enable a higher affinity for the desired drug. Thus, the present study aimed to obtain silica nanoparticles (NPs) doped with low concentrations of europium (III) superficially modified by (3-aminopropyl)triethoxysilane (APTES) to assess their interaction with the model drug cloxacillin benzathine. This drug was chosen because it is part of the ampicillin family and is commonly used in several treatments. Near-spherical and homogeneous silica NPs were obtained via sol-gel synthesis, with particle sizes of approximately 21 nm. It was possible to verify the fluorescence capacity of the silica NPs when doped with europium (III) in a mole percent that varied from 0.5 to 3.0%. A 10% volume percent of APTES caused the silica nanoparticles to increase the degree of hydrophobicity, with a shift in the contact angle from 8° to 51°. After surface modification by APTES, the silica nanocarrier (10 $g \cdot L^{-1}$)

achieved a satisfactory degree of CLOX incorporation (25 $g \cdot L^{-1}$), increasing the adsorptive capacity to values above 50%. Therefore, silica NPs doped with europium (III) in a low percent of 0.5% (mole) modified by APTES showed promising results as an alternative option for trials and clinical studies of drug incorporation.

Keywords: silica; nanoparticles; europium; surface modification; nanocarriers

1. Introduction

Nanoparticles (NPs) have been studied over the years in several areas, especially in the biomedical field, to detect and release drugs in etiologic agents at the cellular level, being applied from diagnosis to treatment [1–3]. Biomedical applications such as anti-cancer drugs, enzymes, and DNA transporters are up-and-coming since they explore the structure of the NPs, which often present a large surface area [4,5]. The size of the synthesized NPs is critical, as studies demonstrate that particles with diameters greater than 100 nm are quickly sequestered by the reticuloendothelial system, accumulating in the liver and spleen before the drug reaches the target cells and tissues. However, smaller NPs (less than 50 nm in diameter) modified with polyethylene glycol (PEG) showed decreased organ sequestration in the reticuloendothelial system, presenting prolonged circulation times [6].

One of the most notable applications is the delivery detection of the asset to the target cells during disease treatments and image mapping in tissues [7,8]. In order to enable the best development of the currently existing techniques, fluorescent NPs have been studied to make sensitive signaling to biological targets. The challenge has been to develop luminescent, non-toxic, and biocompatible nanomaterials that serve as biological markers with good cell visualization and ultra-sensitive immunoassays [9]. Rare earth fluorescent elements are occasionally present in spectroscopic probes for studies of biomolecules and their functions, such as biological targets, immunology, and contrast agents in the non-invasive diagnosis of tissue pathology employing Nuclear Magnetic Resonance (NMR) [10]. These materials combine fluorescence and magnetic resonance to resolve both image resolution and depth and provide a diagnostic tool for *in vitro* and *in vivo* studies, improving the visualization of biological materials and increasing the collected data's credibility.

Furthermore, in biological labeling, these bimodal probes are explored in photodynamic therapy interventions to target tumors and drug carriers. In addition, bimodal probes are of interest to researchers due to their high performance and good biocompatibility [11]. The addition of rare earth elements in nanoparticles assesses structural distortions based on changes in photoluminescent properties [12–16]. Thus, NPs doped with low concentration fluorescent elements are suitable materials for producing bright, attractive imaging labels, particularly for medical diagnosis methodologies that include histology and flow cytometry [17].

A promising candidate for biomedical applications is a silica-based material that presents high monodispersity, stability, and solubility in aqueous solutions even under physiological conditions, in addition to low intrinsic toxicity [18,19] and facilitated methods of surface characterization [20,21]. In its synthetic form, crystalline phases such as quartz, tridymite, and cristobalite can be obtained depending on the temperature, pressure, and degree of hydration employed in the manufacturing

process. In its amorphous form and high reactivity surface, this material presents thermal stability, high surface area, and porous structure. Preparation methods for silica NPs are simple, well known, and some of them, such as the sol-gel method, can be used to synthesize monodispersed silica NPs and produce a wide variety of other ceramic materials [22]. One of the advantages of using silica as a nanocarrier is the possibility of surface modification according to the coveted functionalities, allowing the NPs to interact strongly, in different ways, to a wide variety of biological agents as antibodies, protein complexes, and nucleic acids, among others [23].

In this sense, one of the biological compounds of interest is antibiotics since they are widely used in bacterial treatments and act in several organs of the human body. Thus, the drug delivery control enables drug performance assessments in specific microorganisms and minimizes the use of toxic dosages, improving patient care [24]. Cloxacillin is a beta-lactam antibiotic that belongs to the penicillin family and inhibits bacterial wall synthesis. This medication has numerous clinical indications and is remarkably effective in managing and treating staphylococcal bacterial infections. Therefore, it can be used to treat several conditions, such as pneumonia, urinary tract infections, impetigo, cellulitis, septic arthritis, and wound infections [25–27]. However, the direct applicability of nanocarriers in biological tissues requires a more intense control of the NPs properties through the addition of stabilizers [28,29] and other additives, which may be relevant in future studies based on this paper.

Therefore, the present work aimed to develop luminescent silica nanocarriers doped with europium (III) superficially modified with (3-aminopropyl)triethoxysilane (APTES), an amino-silane compound of great interest in biological molecules. Thus, this work sought to improve luminescent nanocarriers with more remarkable affinities for organic assets that favor drug delivery and biological monitoring.

2. Materials and methods

2.1. Materials

The Sigma Aldrich materials used were 98% tetraethyl orthosilicate (TEOS), ammonium hydroxide solution (NH_4OH), 99% (3-aminopropyl)triethoxysilane (APTES), and 99.9% europium (III) oxide. The cloxacillin benzathine (CLOX, HPLC 97.5%) standard was obtained from Hebei Huari Pharmaceuticals Corporation .The solvents used were 99.5% ethyl alcohol (Vetec-Sigma Aldrich), 99.5% toluene p.a. (Dinâmica), 98.5% sodium phosphate monobasic (NaH_2PO_4, Synth), and sodium phosphate dibasic heptahydrate ($Na_2HPO_4 \cdot 7H_2O$, Synth). All aqueous solutions were prepared with ultrapure water (Milli-Q).

2.2. SiO_2 nanoparticles (NPs) doped with europium (Eu^{3+}) preparation

SiO_2 NPs were synthesized by the previously described Stöber sol-gel method [30]. The reagents TEOS, ethyl alcohol, water, and ammonium hydroxide solution were used to prepare a solution. The solution was kept under constant stirring for 60 min at room temperature and consecutively evaporated until a solid material was obtained. This material was then subjected to heat treatment for 180 min at 350 ºC and 120 min at 400 ºC. In order to obtain the Eu^{3+} doped SiO_2 nanoparticles in the $Si_{1-x}Eu_xO_2$ stoichiometric proportion, 10 mL of a previously prepared solution of

nitric acid (HNO_3) and Eu^{3+} ions (0.5 to 3.0% in weight) from Eu_2O_3 were added to the precursors during the SiO_2 synthesis.

2.3. Silica surface functionalization with (3-aminopropyl)triethoxysilane (APTES)

The SiO_2 NP functionalization aimed to increase the hydrophobic character of the NPs and, consequently, increase their affinity for organic molecules (drugs). For this purpose, the organosilane reagent (3-aminopropyl)triethoxysilane (APTES) was used. The functionalization procedure was adapted from Kresge et al. [31]. For all methods, 0.5 g of the previously dried SiO_2 NP was dispersed in toluene under constant stirring for approximately 1 h at room temperature. Then, the organosilane reagent (APTES), either dispersed or not in the water, was added, and the solution was kept under reflux for 24 h. Subsequently, the material was washed in toluene (no fixed volume) and dried at 80 °C. The specific variations in the volumes of toluene, water, and APTES for each functionalization method are shown in Table 1.

Table 1. Variations in the volumes of toluene, water, and APTES for each functionalization method.

Method	Volume of Toluene (mL)	Volume of Water (mL)	Volume of APTES (mL)
S1	15	-	1
S2	15	-	2
S3	9	1	0.5
S4	18	2	1
S5	9	1	1
S6	8	2	0.5
S7	9.5	0.5	0.5

2.4. Characterizations

Field Emission Gun Scanning Electron Microscopy (FEG-SEM) was used to characterize the size, shape, and distribution of the NPs in a JSM-6701F JEOL® microscope operating at 7 kV. The X-ray diffraction technique (XRD) was used to obtain information on the degree of crystallinity of the NPs. These measurements were performed in a LabX XRD-6000 Shimadzu® equipment using Cu-Kα radiation source (1.5406 Å), at 2θ from 4° to 80° and a scanning step of $1°\cdot min^{-1}$. The specific surface area of the silica NPs was determined by nitrogen adsorption analysis at 77 K in a Micromeritics ASAP-2020 equipment using the Brunauer–Emmett–Teller (BET) method. Fluorescence spectroscopy was performed on the doped silica NPs using a SPEX® 1680 FluoroLog (0.22 m) commercial spectrofluorometer and a Xe lamp (393 nm excitation) in the spectral range from 500 to 700 nm. Luminescence quantum yield analysis was performed according to the procedure described in the literature [32] with sodium salicylate (Sigma-Aldrich, $q = 60\%$) as the quantum yield standard. Fourier Transform Infrared (FTIR) spectroscopy in ATR mode was used to evaluate possible impurities and perform additional structural characterization of the NPs. The spectra were recorded from 400 to 4000 cm^{-1} in a Vertex 70 Bruker® equipment. Nuclear Magnetic Resonance (NMR) spectroscopy measurements of ^{29}Si in solid-state were performed to confirm surface modifications in the functionalized samples in an Avance III HD 400 MHz Bruker® equipment, operating at 10 kHz. From the characteristic chemical displacement (δ) of a given structure, it is possible to identify a sample. The spectra were obtained via simple pulse with high power decoupling (HPDEC), a relaxation time of 10 s, and a pulse length of 5 μs.

Thermogravimetric Analysis (TGA) was used to confirm the presence of APTES in the silica NPs and quantify the percentage of the organic molecule present. The analyses were carried out for the functionalized samples (5 to 10 mg) in STA 409 Netzsch® equipment, in alumina crucibles, at a limit temperature of 900 ºC, under N_2 flow a heating ramp of 10 ºC·min^{-1}. Contact angle measurements were performed to quantify the degree of hydrophobization of the silica NPs after surface modification by APTES. The procedure was carried out in CAM 101 KSV® equipment, with 100 mg of each sample pressed into pellets. A drop of water was deposited on the surface of the samples inside the equipment, and an optical system captured the respective images. The Zeta Potential (ZP) measurements were used to verify the stability and the charge magnitude between the NPs, in a Zetasizer Nano ZS90 Malvern® equipment. For these measurements, approximately 5 mg of the NPs was dispersed in water using an ultrasonic tip for 2 min before each analysis.

2.5. Silica nanocarrier assays: Incorporation and release capacity of CLOX

Adsorption studies were carried out to evaluate the affinity degree of the modified silica NPs with the antibiotic cloxacillin benzathine (CLOX). Initially, 300 mg of the adsorbent materials were added in 30 mL of an aqueous solution containing CLOX (25 mg·L^{-1}), which was then kept under constant stirring (800 rpm) for 24 h at room temperature (25 °C). The suspension was centrifuged, and the supernatant solution was analyzed by UV-Vis Spectroscopy in UV-1601PC Shimadzu® equipment, in the spectral range from 190 to 230 nm. The drug incorporation (mg CLOX g^{-1} silica) of the nanocarriers was calculated based on Eq 1. For UV-Vis spectrophotometry, aliquots were diluted in a phosphate buffer solution (pH 7.4), prepared from a mixture of NaH_2PO_4 (1.2 g), and $Na_2HPO_4{\cdot}7H_2O$ (13.4 g) in 1 L.

$$Drug\ incorporation\ (\text{mg CLOX}\ g^{-1}\ \text{silica}) = \frac{Drug\ free\ in\ solution\ (mg\ L^{-1})}{Drug\ remaining\ in\ solution\ (g\ L^{-1})} \quad (1)$$

In the release assay of the modified nanocarrier incorporated with CLOX, 300 mg of the material was used for 30 mL of a phosphate buffer solution (pH 7.4) in duplicate. After a 24 h exposure of the NPs to the solution under magnetic stirring at room temperature, the suspension was centrifuged and the supernatant was analyzed by UV-Vis spectrophotometry.

3. Results and discussion

The FEG-SEM analysis, shown in Figure 1a, revealed a near-spherical NP morphology and an average size of 21.35 nm (±6.12 nm), shown in Figure 1b, obtained with ImageJ software. The silica average particle size tends to be smaller in basic pH medium (NH_4OH) since the hydrolysis reactions are slower and favor the condensation steps avoiding the undesired increase in the size of silica particles [33]. Therefore, with precise control of the reaction conditions of the Stöber method, it is possible to acquire highly monodisperse NPs with diameters ranging from 15 to 800 nm [34]. Additionally, the nitrogen adsorption analysis by BET method showed that the silica NPs have values of 266.7 m^2·g^{-1} of external surface area, 18.7 m^2·g^{-1} of micropore area, and 58.1 Å of pore size. Thus, homogeneous and porous nanoparticles were obtained through the performed synthesis.

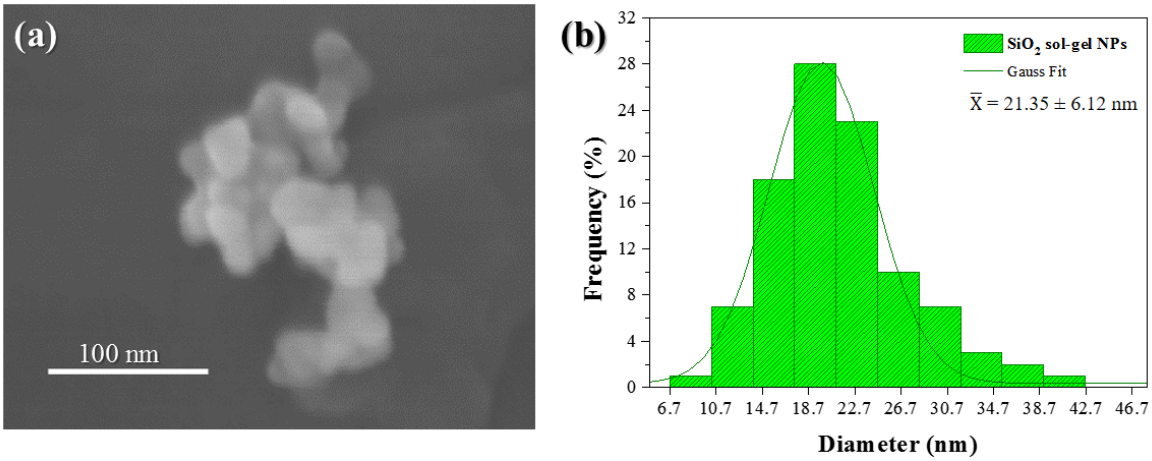

Figure 1. FEG-SEM image of silica sol-gel nanoparticles (a) and their size distribution histogram (b).

The XRD results are shown in Figure 2, in which structural analyses were performed for both pure and Eu^{3+} doped silica NPs. The diffractograms presented an amorphous halo at approximately 23.72°, agreeing with those presented by Syadi et al. [35]. In addition, as described in the methodology section, Eu^{3+} was added in the stoichiometric ratios of $Si_{0.995}Eu_{0.005}O_2$, $Si_{0.99}Eu_{0.01}O_2$, and $Si_{0.97}Eu_{0.03}O_2$, and presented halos in the same positions, without any displacement, as also shown in Figure 2.

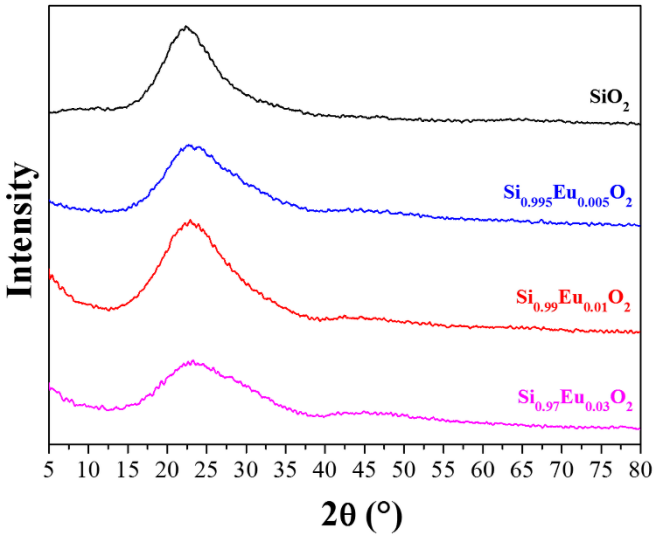

Figure 2. X-ray diffractograms of the SiO_2 NPs and the Eu^{3+} doped SiO_2 NPs in the stoichiometric ratios of $Si_{0.995}Eu_{0.005}O_2$, $Si_{0.99}Eu_{0.01}O_2$, and $Si_{0.97}Eu_{0.03}O_2$.

The transmittance FTIR spectra are shown in Figure 3, in the wavenumber range from 400 to 4000 cm^{-1}. This range is often used to characterize the Si–O–Si vibrational absorption modes, along with phase separation and silicon crystallization from silica-based research [36]. Figure 3

highlights the range of interest from 1600 to 400 cm^{-1} with more details, in which most events are concentrated. All samples presented remarkably similar profiles. The absorption bands in the range between 1110 and 1070 cm^{-1} are correlated to the asymmetric stretching vibration of the siloxane group (Si–O–Si) [37,38]. The absorption band in the range between 815 and 790 cm^{-1} is associated with the Si–O–Si symmetric bond bending vibration [37–39]. The bands between approximately 478 cm^{-1} and 460 cm^{-1} are assigned to the siloxane rocking vibrational mode [37,39]. Therefore, as shown in Figure 3, the Si–O–Si rocking, bending, and stretching vibrational modes are correlated to the adsorption bands at approximately 450 cm^{-1}, 800 cm^{-1}, and 1080 cm^{-1}, respectively [40].

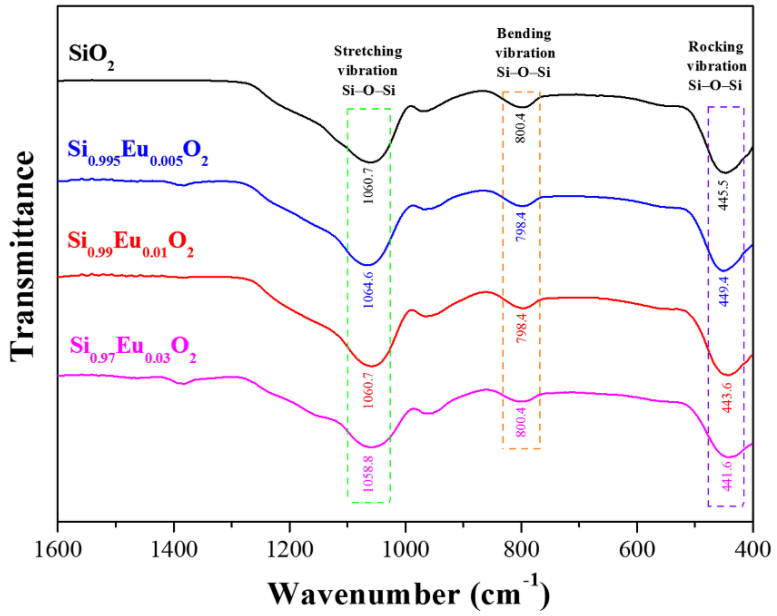

Figure 3. Transmittance FTIR spectra of the SiO_2 NPs and the Eu^{3+} doped SiO_2 stoichiometric NPs ($Si_{0.995}Eu_{0.005}O_2$, $Si_{0.99}Eu_{0.01}O_2$, and $Si_{0.97}Eu_{0.03}O_2$).

Initially, the emission spectrum for the Eu^{3+} doped SiO_2 NPs from $Si_{0.97}Eu0.0_3O_2$ was performed and is presented in Figure 4a. The spectrum shows that the emission is related to the direct excitation of the Eu (III) metal center. The observed result of higher excitation intensity at 392 nm is similar to the Eu^{3+} doped silica reported in the literature [41]. Figure 4b shows the fluorescence emission spectra of the Eu^{3+} doped SiO_2 NPs, with a 392 nm excitation wavelength. These results highlight the Eu^{3+} importance in the presence of luminescence properties in the doped materials. It is possible to observe that all doped samples presented similar profiles and activities with a europium luminescent profile for all $Si_{1-x}Eu_xO_2$ compositions [42]. The emission bands located at 580, 591, and 614 nm are visible even for the lowest Eu^{3+} concentration (0.5% mole percent) [43,44]. Additionally, it is noteworthy that the increase in the Eu^{3+} concentration (up to 3.0% mole percent) caused an increase in the emission intensity, as expected. Thus, the silica NPs doped with the lowest concentration of rare earth europium (III) $Si_{0.995}Eu_{0.005}O_2$ were chosen for the subsequent surface modifications with APTES nanocarrier may be subsequently applied with a low degree of toxicity due to the lower content of the fluorescent element. Additionally, the quantum yield was calculated for the chosen $Si_{0.995}Eu_{0.005}O_2$ NPs and the result was 8.99%, which is consistent with another work

found in the literature for Eu^{3+} doped silica NPs [45] with a similar quantum yield value (7.94% at 255 nm).

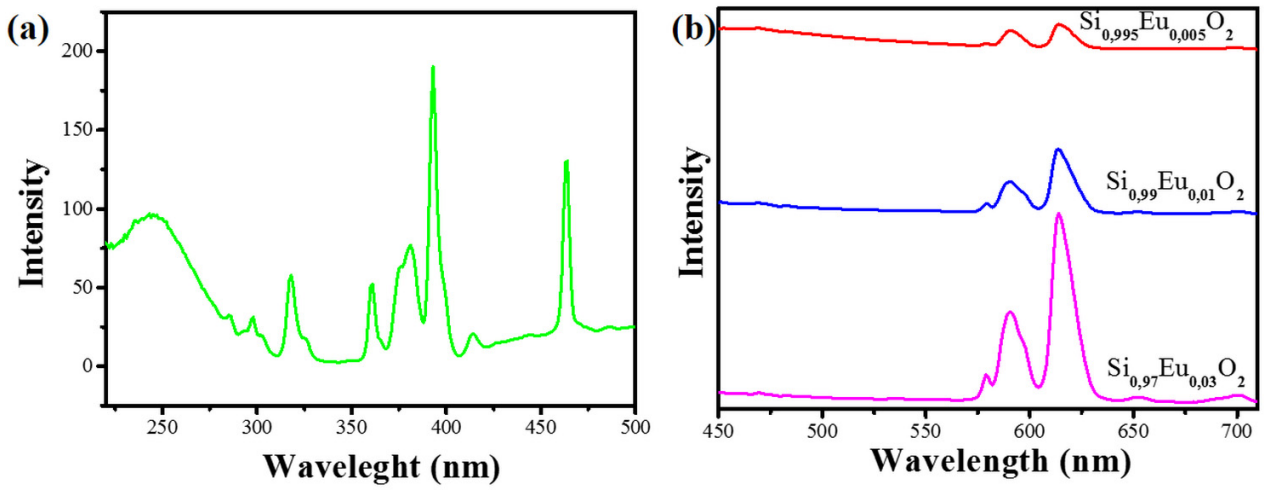

Figure 4. (a) Fluorescence excitation spectra for Eu^{3+} doped SiO_2 and (b) stoichiometric NPs ($Si_{0.995}Eu_{0.005}O_2$, $Si_{0.99}Eu_{0.01}O_2$ and $Si_{0.97}Eu_{0.03}O_2$).

The FTIR spectra, shown in Figure 5, were focused on surface modifications related to APTES. Initially, it is possible to observe that all samples exhibited the characteristic bands of the main vibration modes of the SiO_2 bonds located between 450 and 795 cm^{-1} and correlated to the Si–O–Si symmetrical vibrations. At approximately 955 cm^{-1} is attributed to the presence of Si–OH groups, and the band at 1062 cm^{-1} is associated with the Si–O–Si asymmetric stretching vibrations. All band assignments follow the literature [12]. The FTIR results also suggest the absence of structural or adsorbed contaminants. APTES in the different functionalized silica NPs is correlated to the band around 690 cm^{-1}, which is associated with the asymmetric flexion of O–Si–O [12] and indicates the presence of the organic molecule. It is important to note that the changes were subtle and best evidenced in samples S2, S4, and S5, which indicates that the modification methods were more expressive for the silica NPs with higher APTES content.

Figure 6 presents the thermogravimetric analysis to complete the verification of organic matter residue on the silica surface. TGA weight loss is attributed to the loss of organic matter present on the silica surface. Samples S4 and S5 showed higher weight losses of 22.5% and 22.0%, respectively. Samples S2, S3 and S7 presented weight losses of 17.5%, 12.5% and 12.5%, respectively. Studies in the literature report the importance of a small amount of water to favor modifications [46] instead of large amounts of water, promoting silane polymerization.

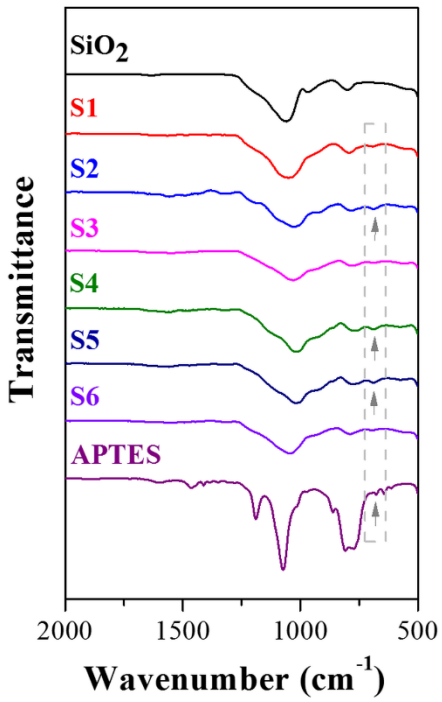

Figure 5. FTIR spectra of sol-gel SiO_2 NPs, functionalized samples S1, S2, S3, S4, S5, S6, and APTES.

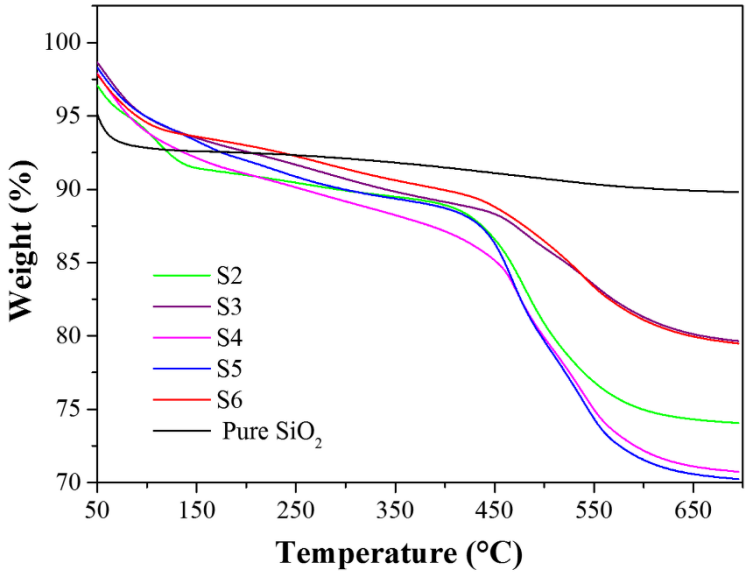

Figure 6. Thermogravimetric analyses of pure sol-gel SiO_2 NPs and functionalized S2, S3, S4, S5, and S6 samples.

The ^{29}Si NMR analysis, shown in Figure 7, was performed to confirm surface modification by APTES, samples before (pure SiO_2), and functionalization (S4 and S5). The pure SiO_2 sample (before APTES functionalization) presented three chemical shifts at −110, −101, and −92 ppm, characteristic of the SiO_2 structure. The signal at −110 ppm is attributed to Q^4 species, with four

siloxane connections (Si–O–Si). The signal at −101 ppm is correlated to Q^3 units, with three siloxane groups and one silanol connection (Si–O–H). The chemical shift at −92 ppm is attributed to Q^2 species with two siloxane and two silanol connections. Both functionalized samples S4 and S5 presented chemical shifts at −67 and −58 ppm, which refer to the modified silica structure due to the substitution of Si–O–H bonds with Si–O–Si–R bonds. These shifts confirm the surface modification of the silica with APTES and corroborate the FTIR data. All chemical shifts observed are in accordance with the values reported in the literature [47] for these materials.

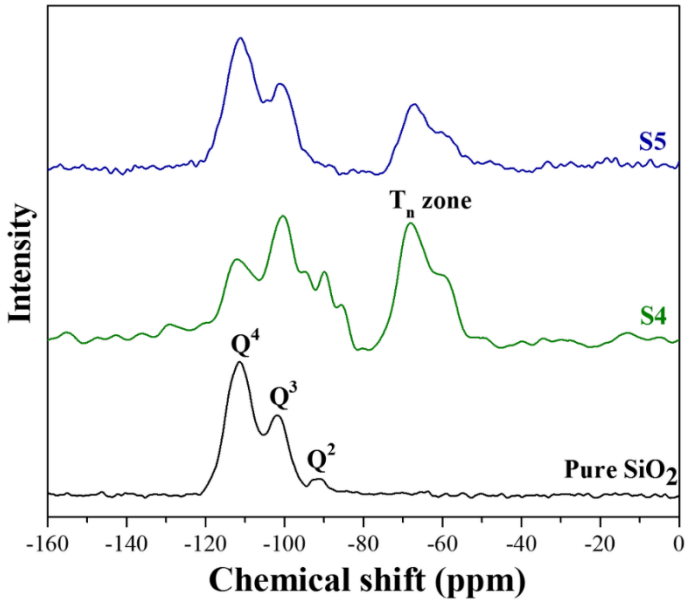

Figure 7. ^{29}Si NMR spectra of pure sol-gel SiO_2 NPs and APTES functionalized silica samples S4 and S5.

Figure 8 illustrates the contact angle measurement used to select the silica with the highest amount of silane on the surface, responsible for the probable increase in hydrophobicity. Figure 8a presented an average angle of 7.88° for pure SiO_2, with high hydrophilicity. Figure 8b,c presented the angles obtained from the surface analysis of the functionalized S4 and S5 samples, with values of 50.98° and 45.36°, respectively. This increase in contact angles verifies the expected increase in hydrophobicity related to the APTES surface modification of the silica [48].

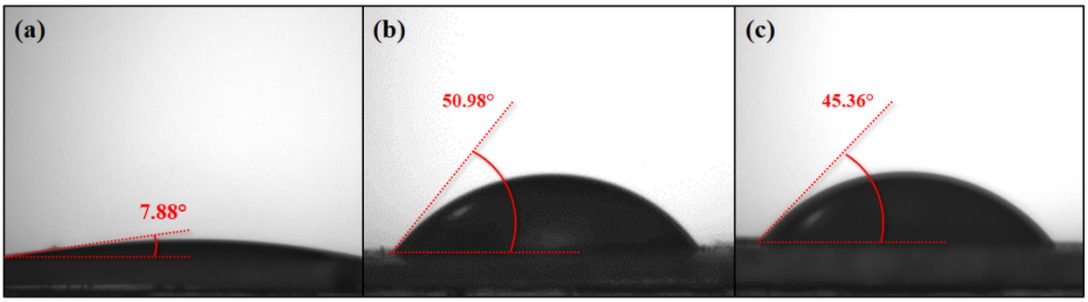

Figure 8. Contact angle images of (a) sol-gel SiO_2 NP, (b) S4, and (c) S5 samples.

The FTIR spectra of silica NPs before and after CLOX incorporation are shown in Figure 9. The characteristic bands of the drug are located at 625 cm^{-1} and in the spectral regions from 1350 to 1710 cm^{-1} and from 3540 to 3780 cm^{-1}. Samples S4 and S5, modified by APTES, were selected for this analysis due to their better interaction with organic molecules (higher hydrophobicities). Figure 9 also shows that the functionalized samples S4 and S5 presented a greater capacity to incorporate the drug when compared to pure SiO_2. Thus, it is possible to infer that the APTES modification was essential to increase the efficiency of the CLOX incorporation.

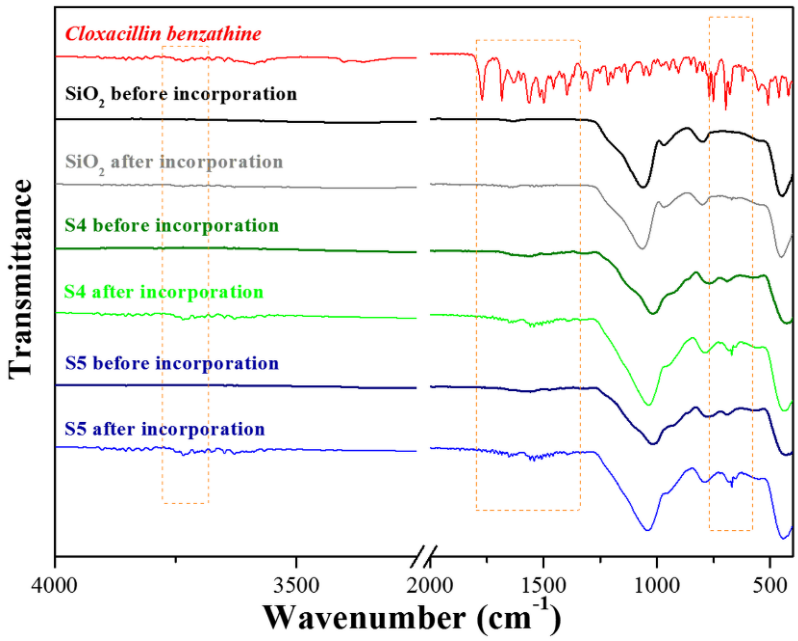

Figure 9. FTIR spectra before and after CLOX incorporation of functionalized samples S4 and S5 and pure SiO_2.

After obtaining the modified ATPES SiO_2 NPs, drug adsorption tests were performed to confirm the effects on the capacity of NPs to incorporate CLOX. Figure 10 shows that the APTES-modified silica NPs (S4) presented almost 50% adsorption superiority compared to pure silica. The greater capacity for CLOX incorporation of the APTES-modified sample is due to its higher affinity for the organic molecules present in the functionalized silica support.

In addition, the drug adsorption capacity, calculated in mg of CLOX divided by g of silica, was 0.8 mg CLOX g^{-1} silica for pure NPs and 1.5 mg CLOX g^{-1} silica for functionalized NPs. These values are correlated with the hydrophobicity of the drug, which makes it difficult to disperse it in an aqueous medium and favors drug adsorption on functionalized silica.

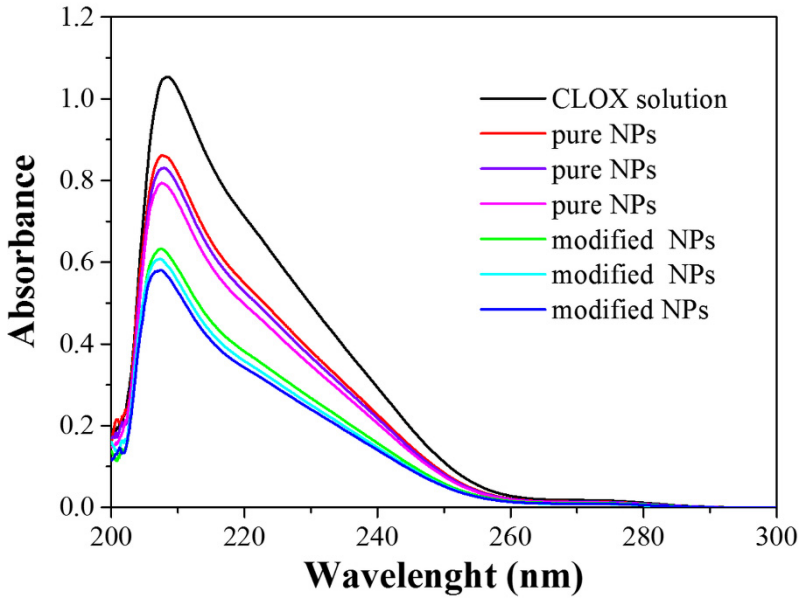

Figure 10. UV-vis spectroscopy related to the adsorption assay of CLOX incorporated by pure SiO_2 NPs and functionalized NPs (S4).

The improved performance of the APTES-modified silica and better affinity due to the presence of organic groups, correlated to their hydrophobic interactions, is attributed to other factors such as electrostatic attraction and hydrogen bonds, which are likely to influence the adsorption process [13–16].

Regarding electrostatic interactions, CLOX has a negative surface charge (−11.40 mV) due to the predominance of four carboxyl groups throughout the molecule, in addition to sulfur and a chlorine atom. The SiO_2 NPs (−22.5 mV) also have a negative surface value, which minimizes the attraction between the silica nanocarrier and the target molecule. Zeta potential analysis (ZP) obtained the surface charge values described in the methodology section. Thus, the inefficiency of the incorporation process for samples that APTES did not modify was corroborated by the non-existent electrostatic attractions between the drug and the silica surface [49]. However, the ZP values obtained for samples modified by APTES are positive (+11.8 mV), which justifies their electrostatic attraction and better drug interaction.

Therefore, it is possible to infer that the APTES modification of the surface has an essential role in the adsorption process for CLOX. The organic groups on the silica surface increase drug interaction and favor the adsorption process [50]. Thus, as observed in Figure 10, the APTES-modified silica nanocarriers became more attractive, enabling better drug incorporation efficiency.

Once the drug was incorporated into the nanocarrier, the aim was to evaluate its release capacity and assess the availability of the antibiotic. Figure 11 shows that, after 24 h of exposure, there was a release of approximately 90 to 95% of the amount initially incorporated into the modified silica NPs, which shows their capability to deliver the drug in a medium that simulates the blood pH. Additionally, the results suggest that the release of CLOX increases after 2 h and achieve a maximum of around 6 h. Thus, APTES-modified silica NPs can become a promising form of drug support since they favor greater transport efficiency and drug-delivering monitoring.

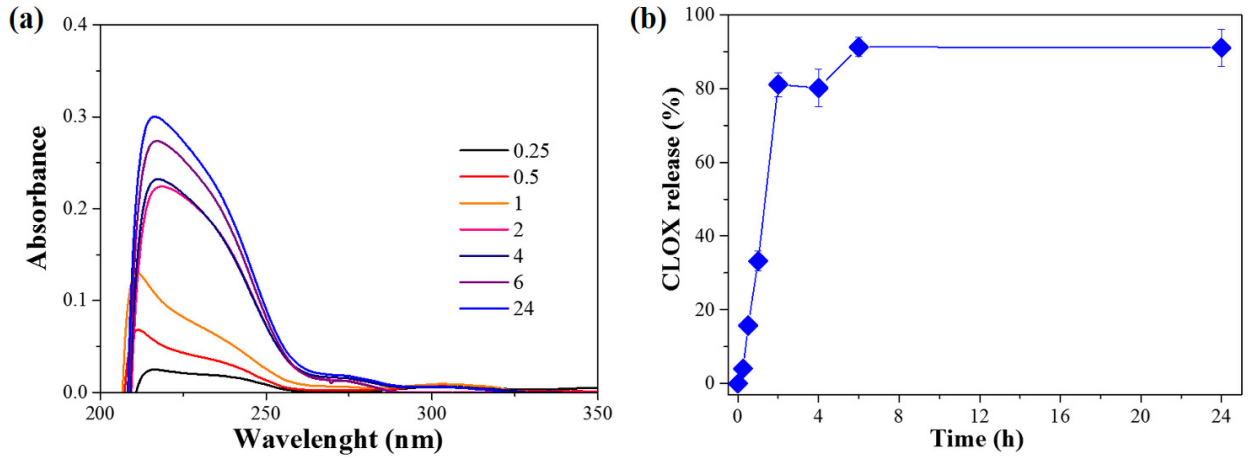

Figure 11. (a) UV-vis spectroscopy of CLOX release by silica NPs and (b) release capacity during 24 h exposure to phosphate buffer solution (pH 7.4).

4. Conclusions

Homogeneous SiO_2 NPs were effortlessly obtained through the sol-gel process and presented a particle size of approximately 21 nm. The structural alteration with doping of europium (III) ions at a low concentration of 0.5% (mole) promoted the silica NPs, previously non-luminescent, to fluorescent materials. The APTES surface modification of the silica NPs was satisfactory, with an increase in the degree of hydrophobicity (contact angle from 7° to 50°), which favored the interaction with organic molecules. The modified NPs enabled a greater degree of CLOX incorporation, with a 50% increase in the ability to adsorb the drug. This increase was attributed to the more significant interaction of the NPs with the organic groups and the change in surface charge, from negative to positive, promoting greater electrostatic attraction between the silica NPs and the drug. Therefore, the silica NPs doped with europium (III) and superficially modified with APTES showed promising results to be applied as a luminescent nanocarrier, with potential drug delivery monitoring through image analysis.

Acknowledgments

The authors acknowledge CNPq (grant n. 461384/2014-0), CAPES (001 Code), Embrapa (grant n. 21.14.03.001.03.00), FINEP, SisNano, and AgroNano Network for their financial support.

Conflict of interest

All authors declare no conflicts of interest in this paper.

References

1. McNamara K, Tofail SAM (2017) Nanoparticles in biomedical applications. *Adv Phys X* 2: 54–88.

2. Becaro AA, Puti FC, Correa DS, et al. (2014) Polyethylene films containing silver nanoparticles for applications in food packaging: Characterization of physico-chemical and anti-microbial properties. *J Nanosci Nanotechnol* 15: 2148–2156.
3. Malafatti JOD, Bernardo MP, Moreira FKV, et al. (2020) Electrospun poly(lactic acid) nanofibers loaded with silver sulfadiazine/[Mg–Al]-layered double hydroxide as an antimicrobial wound dressing. *Polym Adv Technol* 31: 1377–1387.
4. Florek J, Caillard R, Kleitz F (2017) Evaluation of mesoporous silica nanoparticles for oral drug delivery-current status and perspective of MSNs drug carriers. *Nanoscale* 9: 15252–15277.
5. Li Z, Zhang Y, Feng N (2019) Mesoporous silica nanoparticles: synthesis, classification, drug loading, pharmacokinetics, biocompatibility, and application in drug delivery. *Expert Opin Drug Del* 16: 219–237.
6. Gómez-Vallejo V, Puigivila M, Plaza-García S, et al. (2018) PEG-copolymer-coated iron oxide nanoparticles that avoid the reticuloendothelial system and act as kidney MRI contrast agents. *Nanoscale* 10: 14153–14164.
7. Shin K, Choi JW, Ko G, et al. (2017) Multifunctional nanoparticles as a tissue adhesive and an injectable marker for image-guided procedures. *Nat Commun* 8: 1–12.
8. Touloumes GJ, Ardoña HAM, Casalino EK, et al. (2020) Mapping 2D- and 3D-distributions of metal/metal oxide nanoparticles within cleared human ex vivo skin tissues. *NanoImpact* 17: 100208.
9. Liao H, Jiang C, Liu W, et al. (2015) Fluorescent nanoparticles from several commercial beverages: Their properties and potential application for bioimaging. *J Agr Food Chem* 63: 8527–8533.
10. Liu C, Hou Y, Gao M (2014) Are rare-earth nanoparticles suitable for in vivo applications? *Adv Mater* 26: 6922–6932.
11. Yang B, Chen H, Zheng Z, et al. (2020) Application of upconversion rare earth fluorescent nanoparticles in biomedical drug delivery system. *J Lumin* 223: 117226.
12. Lima RC, Espinosa JWM, Gurgel MFC, et al. (2006) Photoluminescence in disordered Sm-doped $PbTiO_3$: Experimental and theoretical approach. *J Appl Phys* 100: 034917.
13. Lima RC, Paris EC, Leite ER, et al. (2007) Structural order-disorder transformations monitored by X-ray diffraction and photoluminescence. *J Chem Educ* 84: 814–817.
14. Gurgel MFC, Paris EC, Souza G, et al. (2007) Jahn-Teller effect on the structure of the Sm-doped $PbTiO_3$: A theoretical approach. *J Mol Struc-Theochem* 813: 33–37.
15. Paris EC, Gurgel MFC, Joya MR, et al. (2010) Structural deformation monitored by vibrational properties and orbital modeling in $(Pb,Sm)TiO_3$ systems. *J Phys Chem Solids* 71: 12–17.
16. Paris EC, Gurgel MFC, Boschi TM, et al. (2008) Investigation on the structural properties in Er-doped $PbTiO_3$ compounds: A correlation between experimental and theoretical results. *J Alloy Compd* 462: 157–163.
17. Mendes AC, Maia LJQ, Paris EC, et al. (2013) Solvent effect on the optimization of 1.54 μm emission in Er-doped Y_2O_3-Al_2O_3-SiO_2 powders synthesized by a modified Pechini method. *Curr Appl Phys* 13: 1558–1565.
18. Croissant JG, Butler KS, Zink JI, et al. (2020) Synthetic amorphous silica nanoparticles: Toxicity, biomedical and environmental implications. *Nat Rev Mater* 5: 886–909.
19. Li Z, Barnes JC, Bosoy A, et al. (2012) Mesoporous silica nanoparticles in biomedical applications. *Chem Soc Rev* 41: 2590–2605.

20. Crucho CIC, Baleiza C, Farinha JPS (2017) Functional group coverage and conversion quantification in nanostructured silica by ^{1}H NMR. *Anal Chem* 89: 681–687.
21. Davidowski SK, Holland GP (2016) Solid-state NMR characterization of mixed phosphonic acid ligand binding and organization on silica nanoparticles. *Langmuir* 32: 3253–3261.
22. Araújo VD, Avansi W, Paris EC, et al. (2011) Influence of pH on the incorporation and growth of Pb_2CrO_5 crystallites in silica matrix. *J Sol-gel Sci Technol* 59: 488–494.
23. Thanh NTK, Green LAW (2010) Functionalisation of nanoparticles for biomedical applications. *Nano Today* 5: 213–230.
24. Gao P, Nie X, Zou M, et al. (2011) Recent advances in materials for extended-release antibiotic delivery system. *J Antibiot* 64: 625–634.
25. Silva R, Martins G, Mario J, et al. (2019) Cloxacillin benzathine-loaded polymeric nanocapsules: Physicochemical characterization, cell uptake, and intramammary antimicrobial effect. *Mater Sci Eng C-Mater* 104: 110006.
26. Hälleberg Nyman M, Johansson JE, Persson K, et al. (2011) A prospective study of nosocomial urinary tract infection in hip fracture patients. *J Clin Nurs* 20: 2531–2539.
27. Bru JP, Garraffo R (2012) Role of intravenous cloxacillin for inpatient infections. *Med Mal Infect* 42: 241–246.
28. Tuomela A, Hirvonen J, Peltonen L (2016) Stabilizing agents for drug nanocrystals : Effect on bioavailability. *Pharmaceutics* 8: 16.
29. Javed R, Zia M, Naz S, et al. (2020) Role of capping agents in the application of nanoparticles in biomedicine and environmental remediation : Recent trends and future prospects. *J Nanobiotechnol* 18: 1–15.
30. Stöber W, Fink A, Bohn E (1968) Controlled growth of monodisperse silica spheres in the micron size range. *J Colloid Interf Sci* 26: 62–69.
31. Kresge CT, Leonowicz ME, Roth WJ, et al. (1992) Ordered mesoporous molecular sieves synthesized by a liquid-crystal template mechanism. *Nature* 359: 710–712.
32. Malta OL, Brito HF, Menezes JFS, et al. (1998) Experimental and theoretical emission quantum yield in the compound Eu(thenoyltrifluoroacetonate)$_{3.2}$(dibenzyl sulfoxide). *Chem Phys Lett* 282: 233–238.
33. Ibrahim IA, Zikry AAF, Sharaf MA (2010) Preparation of spherical silica nanoparticles: Stober silica. *J Am Sci* 6: 985–989.
34. onacchi S, Genovese D, Juris R, et al. (2011) Luminescent silica nanoparticles: Extending the frontiers of brightness. *Angew Chemie Int Edit* 50: 4056–4066.
35. Sayadi K, Rahdar A, Hajinezhad MR, et al. (2020) Atorvastatin-loaded SBA-16 nanostructures: Synthesis, physical characterization, and biochemical alterations in hyperlipidemic rats. *J Mol Struct* 1202: 127296.
36. Koshida N (2008) *Device Applications of Silicon Nanocrystals and Nanostructures*, Springer Science & Business Media.
37. Abadi MHS, Delbari A, Fakoor Z, et al. (2015) Effects of annealing temperature on infrared spectra of SiO_2 extracted from rice husk. *J Ceram Sci Technol* 46: 41–46.
38. Ay F, Aydinli A (2004) Comparative investigation of hydrogen bonding in silicon based PECVD grown dielectrics for optical waveguides. *Opt Mater* 26: 33–46.
39. Bange JP, Patil LS, Gautam DK (2008) Growth and characterization of SiO_2 films deposited by flame hydrolysis deposition system for photonic device application. *PIER M* 3: 165–175.

40. Moore C, Perova TS, Kennedy BJ, et al. (2003) Study of structure and quality of different silicon oxides using FTIR and Raman microscopy, *Opto-Ireland 2002: Optics and Photonics Technologies and Applications*, International Society for Optics and Photonics, 4876: 1247–1256.
41. Selvan ST, Hayakawa T, Nogami M (2001) Enhanced fluorescence from Eu^{3+}-doped silica gels by adsorbed CdS nanoparticles. *J Non-Cryst Solids* 291: 137–141.
42. Shi M, Xia L, Chen Z, et al. (2017) Europium-doped mesoporous silica nanosphere as an immune-modulating osteogenesis/angiogenesis agent. *Biomaterials* 144: 176–187.
43. Volanti DP, Rosa IL V, Paris EC, et al. (2009) The role of the Eu^{3+} ions in structure and photoluminescence properties of $SrBi_2Nb_2O_9$ powders. *Opt Mater* 31: 995–999.
44. André RS, Paris EC, Gurgel MFC, et al. (2012) Structural evolution of Eu-doped hydroxyapatite nanorods monitored by photoluminescence emission. *J Alloy Compd* 531: 50–54.
45. Molkenova A, Oteulina Z, Atabaev TS (2021) Europium (III)-doped mesoporous silica nanoparticles (SiO_2-Eu NPs) prepared via the soaking method. *Results Mater* 11: 100209–100213.
46. Rahman IA, Jafarzadeh M, Sipaut CS (2009) Synthesis of organo-functionalized nanosilica via a co-condensation modification using γ-aminopropyltriethoxysilane (APTES). *Ceram Int* 35: 1883–1888.
47. Bourkaib MC, Gaudin P, Vibert F, et al. (2021) APTES modified SBA15 and meso-macro silica materials for the immobilization of aminoacylases from Streptomyces ambofaciens. *Micropor Mesopor Mater* 323: 111226.
48. Kulkarni SA, Ogale SB, Vijayamohanan KP (2008) Tuning the hydrophobic properties of silica particles by surface silanization using mixed self-assembled monolayers. *J Colloid Interf Sci* 318: 372–379.
49. Wang Y, Sun Y, Wang J, et al. (2016) Charge-reversal APTES-modi fied mesoporous silica nanoparticles with high drug loading and release controllability. *ACS Appl Mater Inter* 8: 17166–17175.
50. Yagub MT, Sen TK, Afroze S, et al. (2014) Dye and its removal from aqueous solution by adsorption: A review. *Adv Colloid Interfac* 209: 172–184.